The Pennsylvania State University

The Graduate School

SIMULATING COMPLEX CO_2 BACKGROUND CONDITIONS FOR INDIANAPOLIS, IN, WITH A SIMPLE ECOSYSTEM CO_2 FLUX MODEL

A Thesis in

Meteorology and Atmospheric Science

by

Samantha Murphy

Submitted in Partial Fulfillment
of the Requirements
for the Degree of

Master of Science

May 2024

The thesis of Samantha Murphy was reviewed and approved by the following:

Kenneth J. Davis
Professor of Atmospheric and Climate Science
Thesis Co-Advisor

Natasha L. Miles
Research Professor of Meteorology and Atmospheric Science
Thesis Co-Advisor

Armen R. Kemanian
Professor of Production Systems and Modeling

Paul Markowski
Distinguished Professor of Meteorology
Head of the Department of Meteorology and Atmospheric Science

ABSTRACT

In this study, we evaluated the ability of a simple ecosystem carbon dioxide (CO_2) flux model, the Vegetation Photosynthesis and Respiration Model (VPRM), to capture the complex CO_2 background conditions observed in Indianapolis, IN. Using simulated biogenic CO_2 fluxes in conjunction with mole fraction tower influence functions, we estimated biogenic CO_2 mole fractions at three background towers in the Indianapolis Flux Experiment (INFLUX) network for three years (April 2017 to March 2020). From the simulated biogenic CO_2 mole fractions, we estimated CO_2 differences between two of the background towers compared to a third tower, which we call CO_2 enhancements. We compared modeled and observed afternoon average CO_2 enhancements at daily and monthly time scales for both towers. We evaluated the random errors introduced by the model for daily, monthly, seasonal, and yearly averaging periods. Additionally, we compared modeled and observed average daily cycles of CO_2 fluxes during the growing season at agricultural eddy covariance flux sites surrounding Indianapolis. Monthly mean model-observation residuals rarely differed significantly from zero (only 7 of 72 site-months), indicating that the model can capture afternoon average CO_2 enhancements at a monthly time scale with no significant bias. We found that the random error was smaller than 1 ppm for monthly, seasonal, and yearly averaging periods. When compared to the average observed daily cycles of CO_2 fluxes during the growing season at corn and soybean sites, the modeled CO_2 fluxes captured the site-to-site differences well. For 9 out of 14 site-months, the modeled maximum afternoon CO_2 drawdown was within 25% of the observed peaks despite the observed maximum drawdowns ranging from -8 μmol $m^{-2}s^{-1}$ to -66 μmol $m^{-2}s^{-1}$. The model had a harder time capturing the peak nighttime respiration, with the modeled peaks differing from the observed peaks by between 22% to 81%. Although not central to our intended application, the model-observation residuals for CO_2 enhancements at a daily time scale were on the same order of magnitude as the observed

enhancements themselves; therefore, the model could not capture the observed day-to-day variations of afternoon average CO_2 enhancements. The results of this study indicate that the simple and computationally inexpensive VPRM can be effectively used in urban CO_2 inversions to represent complex seasonal variations in background conditions observed in Indianapolis. Indianapolis, a modest-size city surrounded by strong ecosystem fluxes, represents a rigorous test for the VPRM system; these results are thus encouraging for the use of VPRM in other urban settings.

TABLE OF CONTENTS

LIST OF FIGURES

LIST OF TABLES

ACKNOWLEDGEMENTS

This work is supported by the National Institute of Standards and Technology (NIST) Project #70NANB19H128. The findings and conclusions in this thesis do not necessarily reflect the views of NIST.

Chapter 1

Introduction

From 2015 to 2020, the contribution of urban areas to total global greenhouse gas (GHG) emissions have risen from an estimated 62% to roughly 70%, with this contribution predicted to increase further through 2050 (Lwasa et al., 2022). Urban areas around the globe are working towards mitigation of climate change and adaptation to its impacts. In recent years, cities have made commitments to addressing climate change and to reducing GHG emissions; efforts include C40 Cites and the Global Covenant of Mayors for Climate and Energy (https://www.c40.org/; https://www.globalcovenantofmayors.org/). However, to assess the effectiveness of these efforts, we must quantify and understand urban GHG emissions.

Urban GHG emissions are quantified using "top-down" or "bottom-up" methods. "Bottom-up", or inventory, estimates are created with accounting-based methods where local activity information, such as traffic data, and models, such as building energy simulations, are combined to quantify the GHG fluxes in the chosen domain (Gurney et al., 2012). Bottom-up emissions estimates can be created at fine spatial (building/road level) and temporal scales with source sectors separated (Gurney et al., 2012). However, bottom-up estimates are often difficult to develop due to limited access to consumption data (Gurney et al., 2012). Additionally, it is difficult to quantify the uncertainties associated with bottom-up emissions estimates (Turnbull et al., 2019). "Top-down" estimates are created using atmospheric observations of GHGs (Verhulst et al., 2017; Miles et al., 2017; Mitchell et al., 2022). There are a variety of platforms used to observe atmospheric GHGs including, but not limited to, satellite, aircraft, building-, and tower-based measurements. In situ urban GHG monitoring networks have been established in a number of cities, including Indianapolis (Davis et al., 2017), Boston (Sargent et al., 2018), Los Angeles

(Verhulst et al., 2017), Salt Lake City (McKain et al., 2012), San Francisco (Shusterman et al., 2016), Toronto (Vogel et al., 2012), Portland (Rice and Bostrom, 2011), Washington, DC/Baltimore (Karion et al., 2020), and Paris (Staufer et al., 2016). These atmospheric observations of GHGs combined with inversion models provide independent methods to assess the accuracy of bottom-up inventory estimates of urban emissions. To estimate spatially and temporally resolved urban emissions, inversion models use a combination of atmospheric GHG observations, atmospheric transport models, and inventory products (Lauvaux et al., 2016; Wu et al., 2018; Turnbull et al., 2019). When solving for carbon dioxide (CO_2) emissions, uncertainties in the spatial structure of prior emissions estimates, atmospheric transport, and biogenic CO_2 fluxes have been shown to poorly impact an inversion's ability to estimate urban emissions (Wu et al., 2018).

Accurate representation of the spatially resolved biological background is critical for inverse estimates of urban anthropogenic CO_2 emissions, especially for cities with significant amounts of vegetation within or surrounding the urban area. Sargent et al., (2018), found that representations of urban biological CO_2 fluxes were necessary for accurate calculations of urban CO_2 emissions using inverse methods during the growing season in the Boston, Massachusetts, region. Lauvaux et al., (2020), found that the estimation of urban emissions calculated using inverse methods in Indianapolis, Indiana, was sensitive to the estimates of biological CO_2 fluxes. Lauvaux et al., (2020), assert that careful estimations of biological CO_2 fluxes are required for accurate calculations of urban CO_2 emissions. A number of studies make use of a simple ecosystem CO_2 flux model, the Vegetation Photosynthesis and Respiration Model (VPRM), to represent biological CO_2 fluxes for urban inversions (e.g., Lauvaux et al., 2020; Wu et al., 2018).

The mole fraction enhancement due to urban GHG emissions can be calculated using in situ tower-based observations of atmospheric GHG mole fractions, but to do so we must separate the enhancements due to local emissions occurring within the urban domain from the GHG mole

fraction of air masses entering the domain (Karion et al., 2021; Turnbull et al., 2015). We refer to the GHG mole fraction of air masses entering the domain as the background. There are a variety of methods, ranging in complexity, that have been applied to separate these signals and calculate the subsequent urban GHG enhancements (Karion et al., 2021). Recent efforts have focused on evaluating the impacts of different background choices on enhancement calculations (e.g., Karion et al., 2021; Miles et al., 2021; Mueller et al., 2018). Mueller et al., (2018), used statistical methods to identify four potential background tower locations outside of the Northeastern Corridor-Baltimore/Washington, DC, area that best capture the variability of CO_2 mole fractions outside of their urban domain. Karion et al., (2021), evaluated a number of methods for representing background CO_2 conditions outside of the Washinton, DC, and Baltimore area, including methods that rely on upwind observations of CO_2 and methods that rely on models. Both of these studies noted the significant impacts of biogenic CO_2 fluxes on background atmospheric CO_2 mole fractions.

Miles et al., (2021), used the Indianapolis Flux Experiment (INFLUX) in situ tower-based GHG observing network to evaluate the impact of background tower choice on the subsequent urban CO_2 enhancement. The authors found that the choice of background tower significantly impacted the calculated urban enhancement. During the growing season, the observed differences in CO_2 mole fraction between three background towers were on the same order of magnitude as the urban enhancements themselves. The authors compared CO_2 mole fraction observations to simple predictions based on landcover types surrounding the towers as well as to estimates created with a more complicated method of using both modeled biological and estimated fossil fuel fluxes. Miles et al., (2021), determined that differing CO_2 fluxes due to vegetation type (forest vs. agriculture) explained some differences in CO_2 mole fraction observations. However, two towers surrounded by the same vegetation type (agriculture) observed significantly different CO_2 mole fractions. Miles et al., (2021), assert that biological

CO_2 fluxes must be quantified and understood to interpret tower-based CO_2 mole fraction measurements in cites surrounded by considerable vegetation.

In this study, we evaluate the ability of a simple ecosystem CO_2 flux model, VPRM, to capture the complex CO_2 background conditions previously observed in Indianapolis (Miles et al., 2021). VPRM's skill in replicating the complex CO_2 background conditions in Indianapolis is of particular interest because of its previous use as a biological prior in CO_2 inversions. Using the simulated biogenic CO_2 fluxes in conjunction with mole fraction tower influence functions, we estimate differences in CO_2 mole fractions between background towers, which we refer to as CO_2 enhancements, using the INFLUX network. We assess the model's ability to capture observed afternoon average CO_2 enhancements at daily and monthly time scales. We also evaluate the random errors introduced by the model for daily, monthly, seasonal, and yearly averaging periods. Further, we test the model's ability to simulate site-to-site differences in CO_2 fluxes using a network of eddy covariance flux towers. This study presents a rigorous method for evaluating biological CO_2 flux estimates that could be applied to any city network that includes multiple background towers.

Chapter 2

Methods

Indianapolis Flux Experiment (INFLUX) Measurement Network

INFLUX is a testbed for developing, evaluating, and improving methods for measuring urban GHG emissions (Davis et al., 2017). INFLUX has quantified urban emissions using a variety of methods, including, but not limited to, tower-based measurements of CO_2 mole fraction, CO_2 flux measurements, atmospheric transport models, aircraft-based measurements, and activity-based GHG inventory products (Davis et al., 2017). Indianapolis, Indiana, is a medium-sized city with an estimated population of about 880,000 people (U.S. Census Bureau, 2022). The city of Indianapolis was chosen as the study site for INFLUX because it is generally isolated from other major GHG sources, it is surrounded by terrain that can be easily simulated by meteorological models, and it is one of the few cities with a high-resolution inventory product available for comparison (Davis et al., 2017).

The in situ communication tower-based GHG mole fraction measurement network consists of fourteen total measurement locations, however, not all locations are currently active. At these sites, wavelength-scanned cavity ring down spectroscopic instruments (Picarro, Inc., models G1301, G2301, G2302, and G2401) measure GHG mole fractions (Miles et al., 2017; Richardson et al., 2017). All 14 tower sites include CO_2 mole fraction measurements, while a subset of them include additional measurements of carbon monoxide and methane (Miles at al., 2017). The CO_2 mole fractions are on the x2019 WMO CO_2 scale and the estimated uncertainty based on flask to in-situ comparisons and round-robin style testing is 0.17 ppm (Richardson et al.,

2017). Locations of the INFLUX CO_2 mole fraction observation towers are shown in Figure 2-1. Further details are documented by Miles et al., (2017) and Richardson et al., (2017).

The INFLUX measurement network also includes eddy covariance CO_2 flux towers that have been deployed at agricultural and urban sites around the city for varying lengths of time. CO_2 eddy covariance flux measurements began at agricultural sites in 2017 and continued to the start of 2023. At these sites, open path CO_2 flux sensors (LI-COR, model LI-7500) measure CO_2 mole fraction and sonic anemometers (Campbell, model CSAT3) measure three-dimensional wind components. These flux measurement sites were located at corn and soybean fields outside of Indianapolis. Locations of CO_2 flux measurement sites in the INFLUX network used in this study are shown in Figure 2-1. For more information about the INFLUX CO_2 flux measurement network see Horne et al., (in prep).

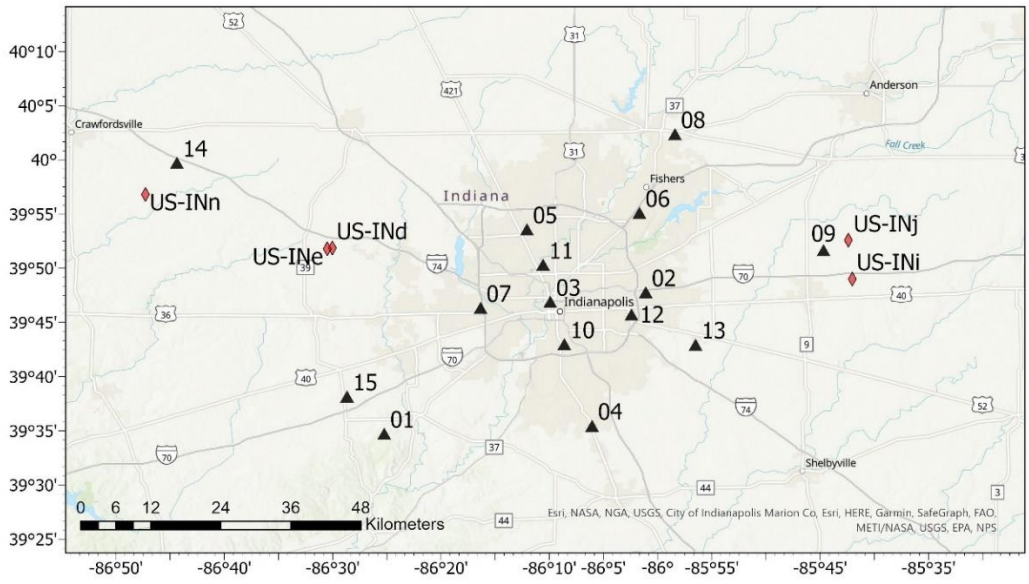

Figure **2-1**: INFLUX CO_2 mole fraction observation tower locations (black triangles) and CO_2 flux measurement sites (red diamonds) located at agricultural fields. Urban CO_2 flux measurements at mole fraction Towers 02, 03, and 07 are not shown.

Modeled Biological CO_2 fluxes with the Vegetation Photosynthesis and Respiration Model (VPRM) and Study Domain

The Vegetation Photosynthesis and Respiration Model (VPRM) is a simple light-use efficiency model which simulates biological CO_2 fluxes (Gourdji et al., 2022). We use the VPRM formulation and parameters from Gourdji et al., (2022), which improves upon the original model structure presented by Mahadevan et al., (2008). VPRM uses parameter sets optimized using eddy covariance CO_2 flux observations to describe different vegetation or land cover types, which are referred to as Plant Functional Types (PFTs). Using VPRM, we calculated Gross Ecosystem Exchange (GEE, the ecosystem's carbon uptake from photosynthesis), ecosystem respiration (R, the ecosystem's carbon release from both autotrophic and heterotrophic respiration), and Net Ecosystem Exchange (NEE), which is the sum of the GEE and R (Gourdji et al., 2022). We implemented VPRM in a roughly 300 km by 300 km domain centered around Indianapolis. The model domain, along with National Land Cover Database (NLCD, Dewitz and U.S. Geological Survey, 2021) land cover information for 2019 and the locations of INFLUX background towers, is shown in Figure 2-2. The model was run at a roughly 1 km^2 spatial resolution and hourly temporal resolution from 2017 through 2021.

VPRM requires a few inputs: Photosynthetically Active Radiation (PAR), air temperature, Enhanced Vegetation Index (EVI), Land Surface Water Index (LSWI), and land cover information (Gourdji et al., 2022). EVI (a greenness index) and LSWI (a moisture index, calculated as a ratio of surface reflectance bands) are remotely sensed gridded products which were obtained from MODIS on the NASA Terra and Aqua satellites (Didan, 2015a; Didan, 2015b; Vermote, 2015a; Vermote, 2015b). We used EVI (MOD13A2/MYD13A2) products at a 1 km grid spacing and aggregated the surface reflectance products (MOD09A1/MYD09A1) used to calculate LSWI from a 500 m grid spacing to a 1 km grid spacing. EVI and surface reflectance products were interpolated from their native temporal resolution to a daily resolution following

the procedure in Gourdji et al., (2022). Air temperature and downward solar radiation were obtained from the Weather Research and Forecasting (WRF) Model (Deng et al., 2017). Temperature and downward solar radiation variables had temporal resolutions of 1 hour and were interpolated from grid spacings of roughly 3 km to roughly 1 km. PAR was calculated from downward solar radiation (Mahadevan et al., 2008). Two 30 m resolution land cover products were used: the Cropland Data Layer (CDL) and the NLCD Imperviousness (USDA NASS; Dewitz and U.S. Geological Survey, 2021). The NLCD Imperviousness product is not available yearly, so the closest available year was used in the model runs (products for 2013, 2016, and 2019 were used). The NLCD Imperviousness product was aggregated to a spatial resolution of roughly 1 km^2. The CDL product corresponding to each year of the model run was used. Using the CDL products, we calculated the fractional area of each model PFT within the approximately 1 km^2 resolution model grid cells. The total GEE, R, and NEE for each grid cell is based on the fractional area of each PFT within the roughly 1 km^2 resolution cells, therefore, we account for the mixture of PFTs within each model cell.

Corn, Other Crops, and Deciduous Broadleaf Forests (DBF) are the dominant PFTs within the model domain. The percentages of each of the nine model PFTs, as well as areas that are missing landcover data or are covered in water, are shown for all years of model runs in Figure 2-3.

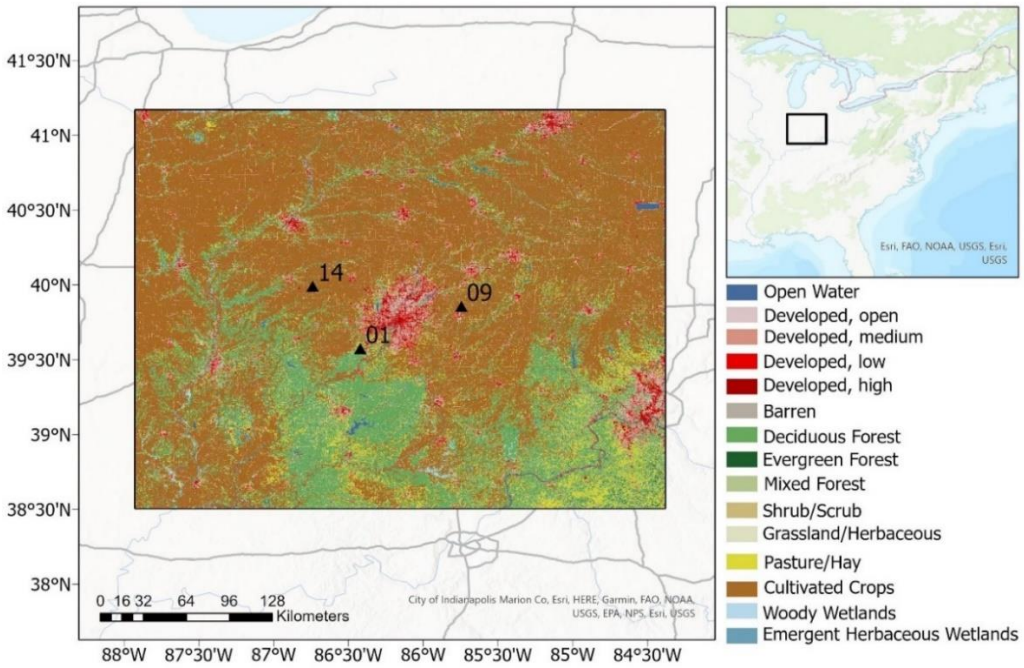

Figure **2-2**: Model domain (black outline) and background towers considered in this study (black triangles) along with National Land Cover Database (NLCD) land cover information for 2019 at a 30 m grid spacing (Dewitz and U.S. Geological Survey, 2021).

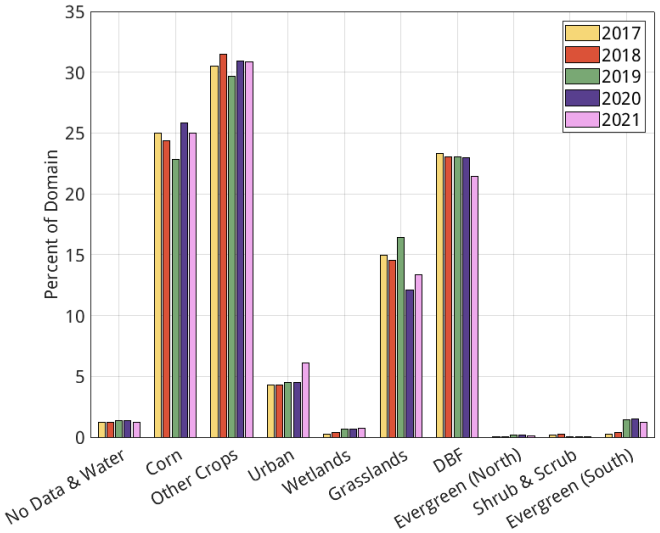

Figure **2-3**: Percentage of each Plant Functional Type (PFT), along with missing data and water, derived from the Cropland Data Layer (USDA NASS) in the model domain for the years 2017 through 2021.

CO_2 Mole Fraction Observations at Background Towers and Enhancement Calculations

This study considered three potential background tower sites in the INFLUX network: Tower 01, Tower 09, and Tower 14. Tower 01 is located on the edge of the DBF southwest of the city (Figure 2-2). Tower 09 is located in an agricultural area east of the city. Tower 14 is located in an agricultural area northwest of the city. Towers 14 and 09 each have one sampling height, 76 m AGL and 130 m AGL, respectively. Tower 01 has multiple sampling heights; we used observations from the highest level, 121 m AGL. CO_2 mole fraction observations (in parts per million, ppm) were averaged to a temporal resolution of 1 hour.

Data points for which any of the three potential background towers are in the urban plume, i.e., downwind of the urban area, were excluded from the analysis. Following Miles et al., (2021), data points were excluded when the wind directions were 20° to 65° or 235° to 280°. Wind direction data were obtained from two Automated Surface Observing Systems stations, IND and EYE, which are located at airports within the model domain (https://www.weather.gov/asos/). Wind data at the end of each hour at the IND station was selected to represent the wind direction for each hour. Hours missing wind direction data in the IND data set were filled with data from the EYE station, if available. We additionally excluded CO_2 mole fraction data points from all towers for any hour during which any one of the three towers was missing wind direction or CO_2 mole fraction observations.

The enhancement, i.e., the difference of CO_2 mole fractions between the background towers was calculated. Note that the enhancement in this case does not represent the impact of urban emissions, instead it represents spatial structure in the background mole fraction values. This enhancement can be either positive or negative. We calculated hourly enhancements for Towers 01 and 14, with respect to Tower 09. Note that in this analysis we compared CO_2 mole

fractions across towers at the same time of day, which is consistent with past INFLUX studies (e.g., Miles et al., 2017). In this study, we focused on observations from April 27, 2017, through March 9, 2020. This period was chosen because all three background towers were operational, and we wanted to exclude any times where observations could be impacted by the COVID-19 lockdowns beginning in March 2020 (King, 2021).

We focused our analysis of CO_2 enhancements on afternoon average enhancements, where afternoon hours are defined as 1700-2200 UTC (1200-1700 LST). One reason we focus on afternoon hours is that the atmospheric boundary layer is typically well mixed during this time, making interpretation of measurements simpler (e.g., Bakwin et al., 1998; Miles et al., 2017). Note that the afternoon enhancements are affected by fluxes in the domain several hours prior to the tower measurement time.

Modeled Biogenic CO_2 Mole Fractions for Background Towers and Enhancement Calculations

In order to test VPRM's ability to simulate the spatial and temporal structure in background CO_2 mole fractions, we estimated the biogenic contribution to total CO_2 mole fraction at each of the three background towers by convolving VPRM NEE outputs, which represent the surface biogenic CO_2 fluxes, with tower influence functions. The influence functions were generated with a Large Particle Dispersion Model (Uliasz, 1994) using WRF input data (Deng et al., 2017) for the three background towers for a roughly 300 km by 300 km domain around Indianapolis with a grid spacing of 3 km. The influence functions used account for surface impacts in the 72 hours prior to the observation hour. Before convolving with the tower influence functions, VPRM NEE estimates were aggregated to a grid spacing of roughly 3 km to match the influence function resolution. Note that the CO_2 mole fraction estimates resulting from this

convolution can be positive or negative because they represent only the biogenic contribution to the total CO_2 mole fraction at each tower.

We calculated the modeled biogenic contribution to CO_2 mole fraction at each background tower from April 27, 2017, through March 9, 2020. From this, we calculated the model-predicted enhancement between towers as for the observed enhancements.

Estimation of Total Tower Influence and Plant Functional Types within Tower Influence

We determined the dominant PFT within the surface area influencing each of the towers by calculating the total afternoon influence due to Corn, Other Crops, and DBF for Towers 01, 09, and 14 during the month of July 2018. July 2018 was chosen as a representative growing season month. Further, we evaluate differences in total surface influence for each of the towers by calculating the total influence during the afternoon in July 2018. To calculate the contribution to the total influence from each PFT, we convolved the influence functions for each tower with a map representing the fractional area of the PFT of interest within each approximately 3 km grid cells. To calculate the total influence for each tower, we summed the influence functions over time (72 hours back in time) and space. For these calculations, we consider only afternoon hours during which we had an associated mole fraction observation.

Model-Observation Comparison: Afternoon Average CO_2 Enhancements

To evaluate VPRM's ability to represent the complex background CO_2 conditions observed, we compared the observed afternoon average CO_2 mole fraction enhancements for Towers 01 and 14 to the modeled afternoon average enhancements and assessed model performance at multiple time scales. We compared modeled and observed enhancements at each

tower because we modeled only the impacts of biological fluxes on the CO_2 mole fraction within the model domain (Figure 2-2), and not the total mole fraction. To model total CO_2 mole fraction, anthropogenic CO_2 sources and inflow from outside of the domain would also need to be considered. Our approach assumes that the impact on CO_2 mole fraction from outside the model domain (Figure 2-2) is nearly uniform across the towers; we assert that the major differences in biogenic CO_2 influence on the background towers are contained within the model domain. We calculated modeled and observed afternoon average CO_2 enhancements at Towers 01 and 14 for each day in the time series, along with the associated residuals, where the residual is the modeled minus the observed value for each afternoon average enhancement. We calculated the mean monthly afternoon average enhancements, the mean monthly residuals, and the associated standard errors of the residuals for Towers 01 and 14 for every month in the time series considered. Additionally, we evaluated the impact of averaging time period length on random error magnitude by calculating the mean absolute error of the residuals for daily, monthly, seasonal, and yearly averaging periods. For this calculation of mean absolute error of the residuals, we include the residuals for both Towers 01 and 14 in the same data pool.

Depletion in Atmospheric CO_2 Mole Fraction Due to Individual Plant Functional Types

In order to assess the impacts of individual PFTs on total CO_2 drawdown, we estimated the contribution of Corn, Other Crops, and DBF to the total biogenic CO_2 mole fractions, which we refer to as the depletion in CO_2 mole fraction caused by the individual PFTs, at Towers 01, 09, and 14 for the month of July 2018. We performed a similar convolution to that discussed in the section titled Modeled Biogenic CO_2 Mole Fractions for Background Towers and Enhancement Calculations, however instead of performing the convolution using total modeled NEE for each grid cell, we used NEE estimates for Corn, Other Crops, and DBF PFTs separately.

This allowed us to calculate the afternoon average biogenic depletion in CO_2 mole due to each PFT at each tower. Then, we computed the average biogenic depletion in CO_2 mole from each PFT over all afternoons during the month.

Net Ecosystem Exchange (NEE) for Plant Functional Types within Tower Influence Functions

In order to assess productivity gradients across towers, we calculated the predicted productivity, i.e., CO_2 drawdown as predicted by NEE, of Corn, Other Crops, and DBF PFT categories within the influence functions of each tower for the month of July 2018. For this analysis, we performed a similar convolution to what was described in the previous section, however, in this case we do not account for the fractional area of each PFT in each grid cell. This allowed us to directly evaluate predicted productivity differences in vegetation surrounding each tower. We calculated the afternoon average NEE for each tower and PFT combination and then the mean of afternoon averages over the month of July 2018.

Rural CO_2 Flux Observations and Vegetation Fraction Filtering

In this study, we evaluated VPRM's ability to simulate site-to-site difference in CO_2 fluxes at agricultural sites using observations from the INFLUX network. For this evaluation, we considered CO_2 flux observations at five agricultural sites in the model domain between the years 2017 and 2021. These flux sites are summarized in Table 2-1. All flux towers considered had a measurement height of 3 meters AGL.

CO_2 flux data were subject to a quality control process (Horne et al., in prep). CO_2 flux observations were filtered using tests from Vickers and Mahrt (1997) and Foken (2008).

Additionally, we removed data when the friction velocity falls below a threshold value determined for each site.

CO_2 flux observations were filtered to remove points when less than 90% of the flux footprint area was attributable to the vegetation type of interest. For this study, the vegetation of interest was either corn or soybean. We used the Flux Footprint Prediction (FFP) model by Kljun et al., (2015), to assess the fractional coverage of soy or corn within each half-hourly flux measurement. We used imagery from Google Earth and ArcGIS Pro software to visually select areas covered with the vegetation of interest. Areas with the vegetation type of interest were assigned a value of 1 while other areas were assigned a value of zero. For all half hours during which the required input data was available, we used the FFP climatology function to simulate footprints at a 1 m grid spacing for a 501 m by 501 m domain. We multiplied the simple site map that indicates landcover type with a footprint estimate to obtain a gridded map representing only the footprint attributable to the vegetation of interest. For every possible half hour, we computed two values using the predicted footprints: a value representing the footprint attributable to the vegetation of interest and a value for the total footprint. The former was calculated by summing over the footprint attributable to the vegetation of interest and the latter was calculated by summing the footprint over the entire domain. The ratio of these values represented the fraction of the footprint attributable to the vegetation of interest. We removed CO_2 flux data points when this fraction was less than 0.90, i.e., when less than 90% of the predicted half hourly flux footprint was attributable to the vegetation of interest. Additionally, we removed CO_2 flux data points when the fraction was not able to be calculated.

Table **2-1**: Summary of CO_2 flux measurement sites in the Indianapolis Flux Experiment (INFLUX) network used in this study along with vegetation types for each site during the growing season.

SITE NAME	YEARS	VEGETATION TYPES
US-INd	2018	Soybean
US-INe	2018	Corn
	2019	Soybean
	2020	Corn
US-INi	2019	Soybean
US-INj	2020	Corn
US-INn	2019	Corn
	2021	Corn

Model-Observation Comparison: Agricultural CO_2 Fluxes

To evaluate VPRM's ability to simulate agricultural CO_2 fluxes, we compare the mean modeled daily cycle of CO_2 fluxes, or NEE, to the mean observed daily cycle during the growing seasons months of July and August. Using the filtered flux data, we created hourly data sets from our half hour interval flux observations by averaging the two points within the hour. Observed fluxes from sites with corn are compared to modeled fluxes from the Corn PFT. Because there is no specific soybean PFT in our VPRM formulation, fluxes from sites with soybean are compared to modeled fluxes from the Other Crops PFT. For each site-month, for any hour when there was no observed CO_2 flux, the corresponding NEE point was also removed. We calculated mean daily cycles of observed CO_2 flux during July and August, separately, of each year. We compared the peak CO_2 drawdown and peak respiration estimated by the model to the observation in order to assess the model's ability to capture observed agricultural CO_2 fluxes.

Chapter 3

Results

Model-Observation Comparison: Afternoon Average CO_2 Enhancements

There is large day to day variation in both the modeled and observed afternoon average CO_2 enhancements for Towers 01 and 14 (Figure 3-1a,b). There is also a seasonality in the magnitude of the enhancements for both Towers 01 and 14. The observed enhancements at both towers tend to be larger in magnitude during the growing season than during the dormant season. Observed enhancements have magnitudes as large as 20 ppm. The modeled enhancements at both towers also tend to be larger during the growing season than during the dormant season. However, the modeled enhancements tend to be smaller in magnitude and exhibit less variation compared to the observations during the dormant season.

The model is not able to capture the observed afternoon average CO_2 enhancements on a daily time scale. For both Towers 01 and 14, the residuals (model – observations) are the same order of magnitude as the enhancements themselves (Figure 3-1c,d). During both the growing and dormant seasons, the magnitude of the residuals can be as large as 20 ppm.

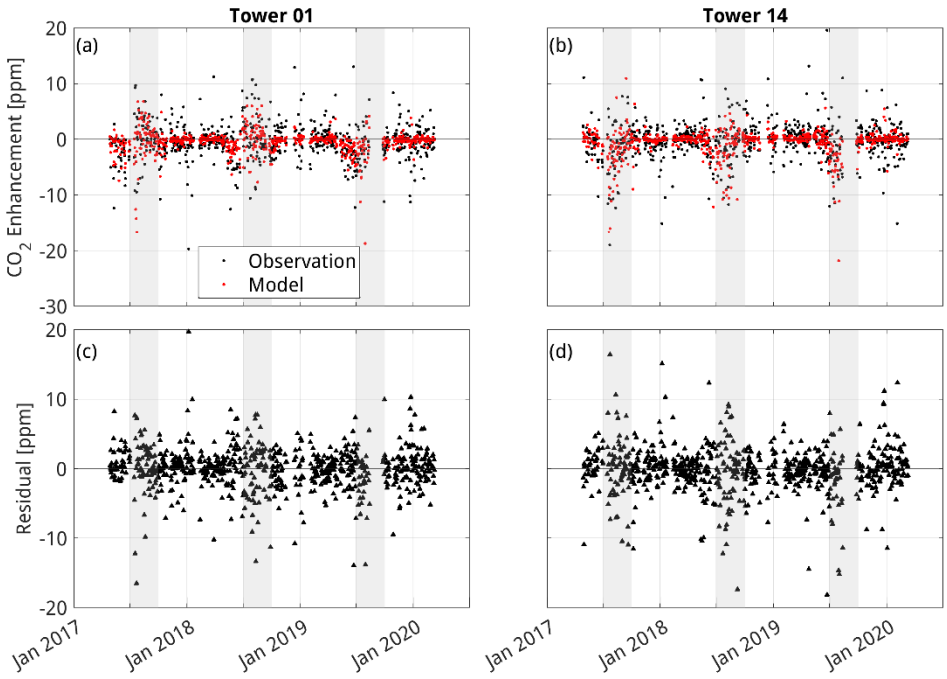

Figure **3-1**: Observed (black circles) and modeled (red circles) afternoon average CO_2 enhancements relative to Tower 09 at Towers 01 (a) and 14 (b) between April 27, 2017, and March 9, 2020. Residuals (model-observation) for the afternoon average CO_2 enhancements at Towers 01 (c) and 14 (d) for the same time period. Gray shading indicates July through September.

More important for the application of top-down urban emissions determination, the model captures the timing and magnitude in afternoon average CO_2 enhancements at Towers 01 and 14 when averaged over each month (Figure 3-2). Forested areas surrounding Tower 01 green up prior to the agricultural vegetation near Tower 09, resulting in persistent negative enhancements in June, both observed and modeled. During the peak of the growing season, the drawdown from the agricultural vegetation near Tower 14 is larger than that near Tower 09, again resulting in negative observed enhancements that the model correctly predicts. CO_2 residuals do not differ significantly from zero for most months in the time series considered, as indicated by the zero falling within two times the standard error of the monthly mean residual for most months. For Tower 01, 3 months (June 2017, January 2018, and July 2019) have residuals significantly different from zero and for Tower 14, 4 months (June 2017, January 2018, May

2018, and December 2019) have residuals significantly different from zero. Therefore, for most site-months considered, the modeled enhancement is not significantly different from the observed enhancement. For Tower 01, 28 out of 36 months have residuals less than 1 ppm and 27 out of 36 months have residuals less than 0.5 ppm. For Tower 14, 25 out of 36 months have residuals less than 1 ppm and 29 out of 36 months have residuals less than 0.5 ppm. From this, we conclude that there is no seasonal bias and that the model error is random.

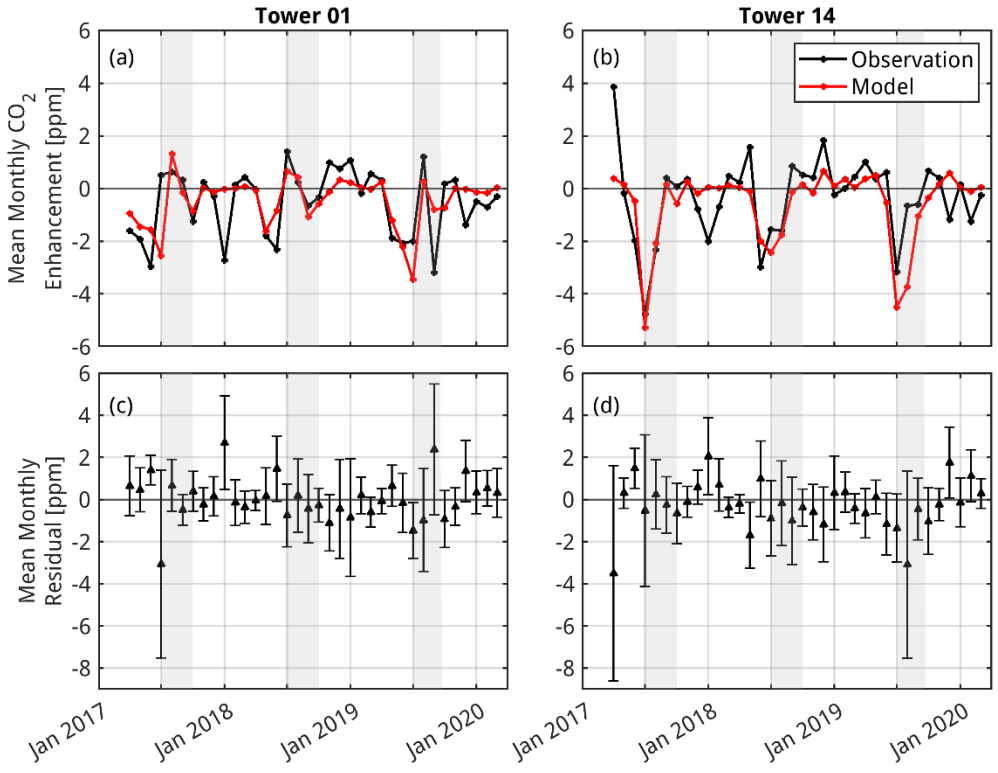

Figure **3-2**: Observed (black) and modeled (red) monthly mean afternoon average CO_2 mole fraction enhancements compared to Tower 09 for Towers 01 (a) and 14 (b) and the monthly mean afternoon average model-observation residuals (black triangles) for Towers 01 (c) and 14 (d) starting April 2017 and ending March 2020. Error bars are two times the standard error. Gray shading indicates July through September.

The magnitude of the typical random error, as represented by the mean absolute error of the residuals, decreases with increasing averaging periods (Figure 3-3). Note that the residuals here still refer to the difference between modeled and observed afternoon average CO_2

enhancements. The largest decrease in random error occurs when increasing the averaging period from a day to a month; the random error decreases by about 1.4 ppm if a month is chosen as the averaging period compared to a day. Increasing the averaging period to a season or year results in additional decreases in random errors, with both averaging periods resulting in random errors of less than 0.5 ppm.

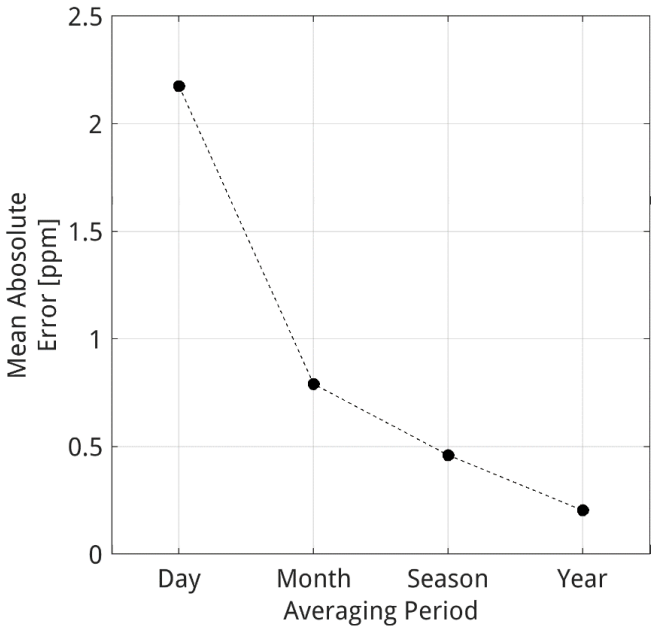

Figure **3-3**: Mean absolute error of model-observation residuals calculated for daily, monthly, seasonal, and yearly averaging periods for both Towers 01 and 14 combined.

Depletion in Atmospheric CO_2 Mole Fraction Due to Individual Plant Functional Types

The average estimated depletion in atmospheric CO_2 mole fractions due to Corn, Other Crops, DBF, and all PFTs combined during the month of July 2018 vary in magnitude across background towers (Figure 3-4). The model total (i.e., all PFTs combined) magnitude of depletion in CO_2 mole fractions caused by biology at Tower 14 is approximately 30% larger than

the same depletion at Tower 09 and approximately 40% larger than the depletion at Tower 01. This indicates that, on average, there is a larger drawdown of CO_2 within the area of influence at Tower 14 compared to the other two towers. Most of the modeled difference in CO_2 depletion for Tower 14 compared to Tower 09 results from the difference in the drawdown by corn. However, this calculation does not distinguish between differences in the area of corn landcover versus more vigorous growth.

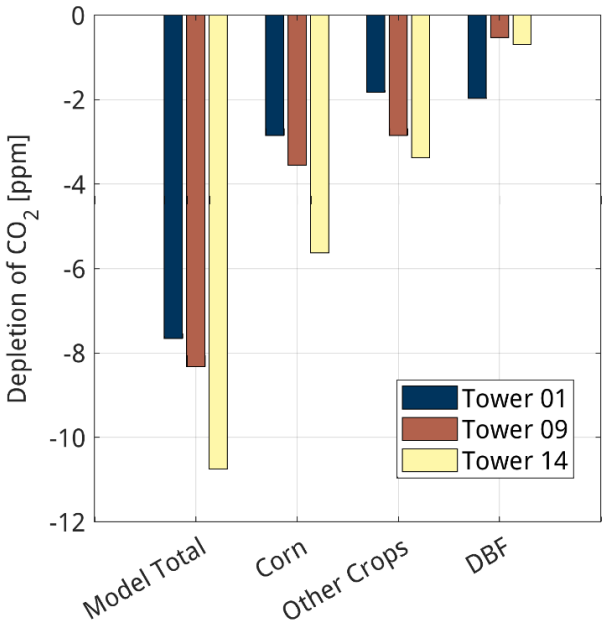

Figure **3-4**: Afternoon average atmospheric CO_2 mole fraction depletion due to biogenic CO_2 fluxes from Corn, Other Crops, and Deciduous Broadleaf Forest (DBF) Plant Functional Type (PFT) categories as well as the model total (all PFTs combined) predicted CO_2 depletion for Towers 01, 09, and 14 averaged for the month of July 2018.

Estimation of Total Tower Influence and Plant Functional Types within Tower Influence

Corn and Other Crop PFT categories dominate the influence functions for Towers 09 and 14, while the DBF PFT category dominates the influence function for Tower 01 during afternoon

hours of July 2018 (Figure 3-5). The relative influence of Corn, Other Crops, and DBF generally matches qualitative expectations based on the locations of the towers (Tower 01 has the most influence from DBF while Towers 09 and 14 have most influence from Other Crops and Corn). Tower 09 has the largest magnitude of influence, with Towers 14 and 01 following in magnitude. Because the total influence of Tower 09 is greater than that of Tower 14 during the afternoon hours, the greater drawdown observed at Tower 14 cannot be attributable to the difference in total influence between the two towers. Additionally, the corn contribution to the influence functions for Towers0 9 and 14 are similar and the other crops contribution is not different enough to explain the observed difference in CO_2 drawdown at these agriculturally dominated towers.

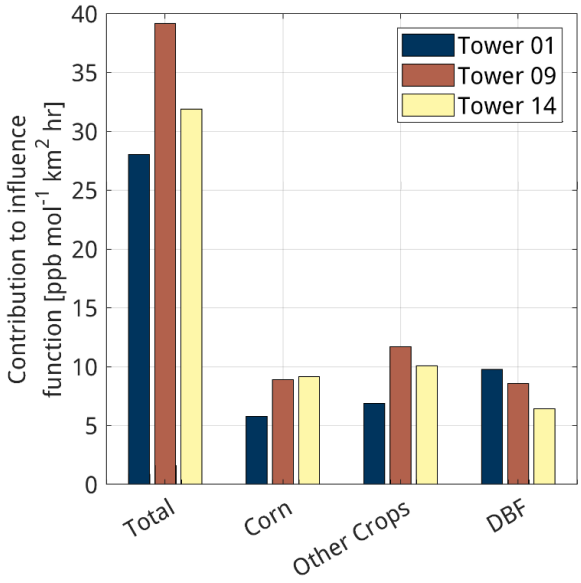

Figure **3-5**: Contribution of Corn, Other Crops, and Deciduous Broadleaf Forests (DBF) Plant Functional Type (PFT) categories to the total influence as well as the total influence for Towers 01, 09, and 14 during the afternoon hours of July 2018. Units are the same as those of the influence functions. Note that the sum of the influence for the three PFTs considered here does not equal the total summed influence for any tower because the surface area within the influence functions contains additional PFTs that are not considered here.

Net Ecosystem Exchange for Plant Functional Types within Tower Influence Functions

During July 2018, VPRM suggests that the vegetation upwind of Tower 14, regardless of PFT, is more productive than the vegetation upwind of Towers 01 and 09 (Figure 3-6). Tower 01 has the next most productive vegetation upwind, and Tower 09 has the least productive vegetation upwind. This indicates that the larger magnitude of CO_2 mole fraction depletion from Corn at Tower 14 is due to the higher predicted productivity. Across all towers, Corn is the most productive PFT, followed by Other Crops, and then followed by DBF. This is consistent with our understanding of these ecosystems and previous results (e.g., Miles et al., 2021).

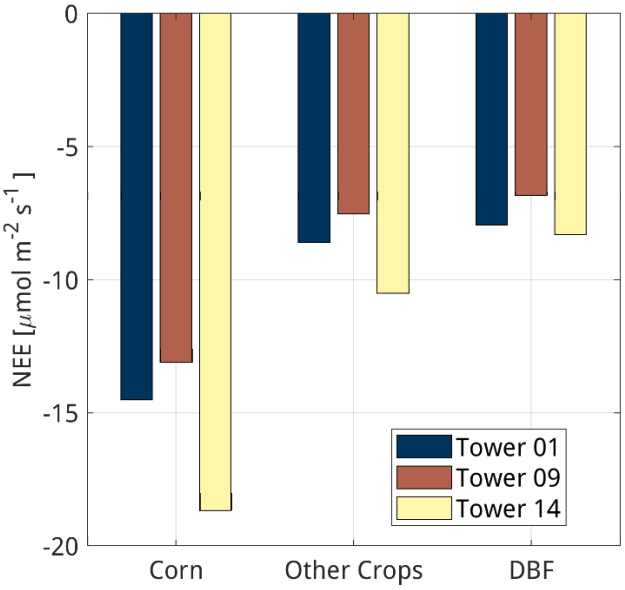

Figure **3-6**: Afternoon average Net Ecosystem Exchange (NEE) within influence functions for Corn, Other Crops, and Deciduous Broadleaf Forest (DBF) Plant Functional Types (PFTs) for Towers 01, 09, and 14 averaged for the month of July 2018.

Model-Observation Comparison: Agricultural CO_2 Fluxes

We have shown that VPRM is able to predict the differences in CO_2 mole fraction enhancements at INFLUX background towers and now we further show that VPRM captures the site-to-site variability in the observed daily cycle of CO_2 fluxes during the months of July and August (Figure 3-7). Across all the site-months, the modeled peak in afternoon CO_2 drawdown was between 4% to 56% of the observed peak. The model had the most trouble capturing the CO_2 drawdown at the site US-INn during July 2019, when the model differed from the observed peak drawdown by 56% and the peak respiration by 67%. For 9 out of 14 site-months, the modeled peak afternoon CO_2 drawdown was within 25% of the observed peak despite the observed peaks ranging from -8 μmol $m^{-2}s^{-1}$ to -66 μmol $m^{-2}s^{-1}$. The model had a harder time capturing the peak respiration, with the model peak differing from the observed peak by between 22% to 81%. The observed peak respiration varied across site-months from 4.1 μmol $m^{-2}s^{-1}$ to 40 μmol $m^{-2}s^{-1}$. Additionally, there does not appear to be a difference in the model's ability to capture the observed trends in the CO_2 drawdown for either corn or soybeans.

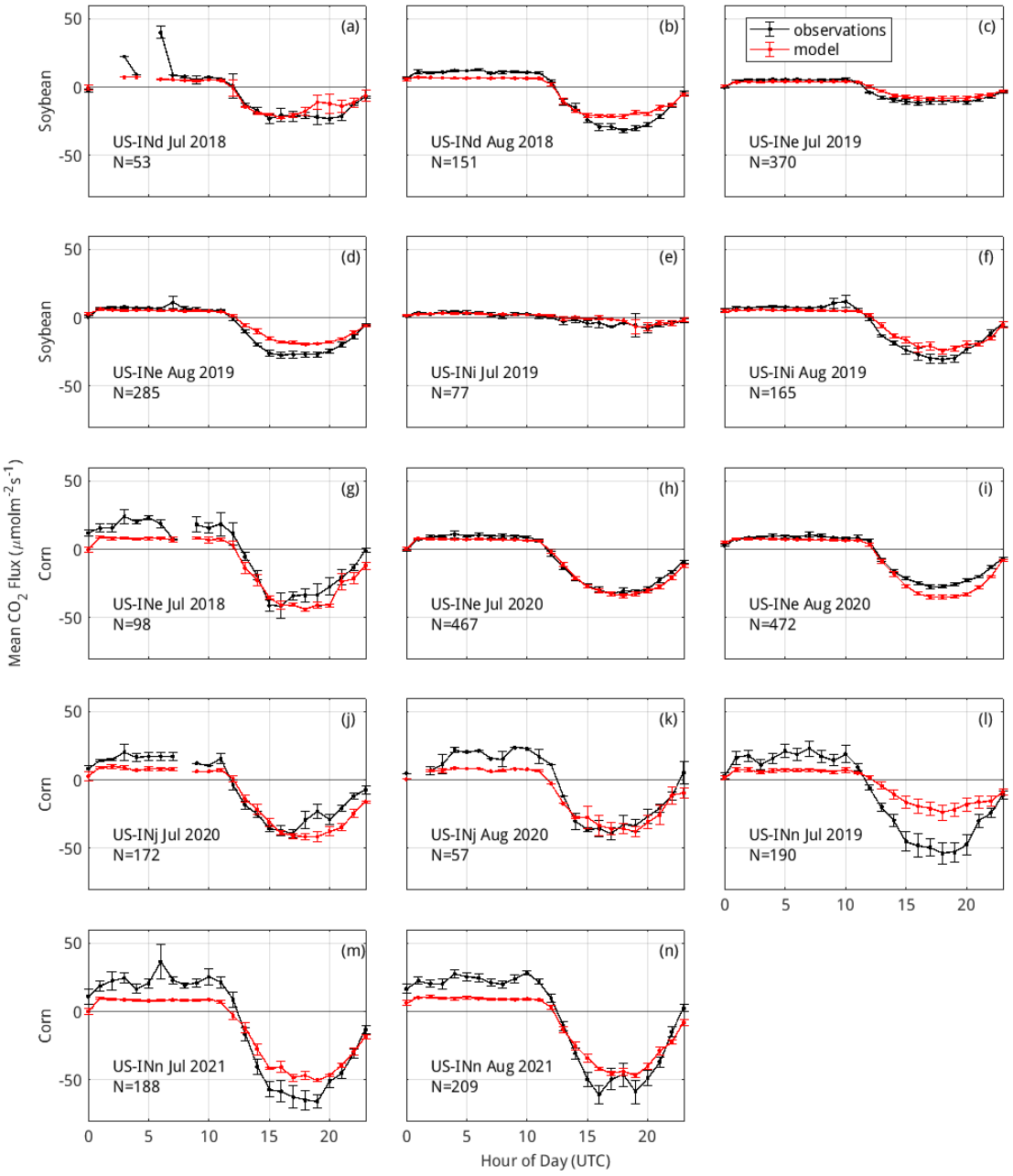

Figure **3-7**: Mean daily cycles of CO_2 fluxes calculated over July and August for each site and year. Observations are shown in black and model outputs are shown in red. Time in UTC. Error bars indicate the standard error. The top two rows (a, b, c, d, e, f) are soybean sites (Other Crops Plant Functional Type in model), the following rows (g, h, i, j, k, l, m, n) are corn sites. Site names, year and month, and number of points included in the cycle average are indicated on each panel.

Chapter 4

Discussion

With monthly or longer averaging periods, VPRM is able quantify differences in CO_2 mole fraction between background towers at a level sufficient for use in urban enhancement calculations. Overall, we have shown that differences between the modeled and observed CO_2 enhancements are random, and not a result of model bias. Miles et al., (2021), found that average urban CO_2 enhancements were on the order of 3-5 ppm in Indianapolis (calculated during the dormant season using urban Tower 03 and background Tower 09 in the INFLUX network). A central goal of the INFLUX project is to quantify urban GHGs in Indianapolis with an accuracy of 10% or less (Davis et al., 2017). In order to quantify average Indianapolis urban enhancements within 10% accuracy, we aim to quantify CO_2 enhancements with less than roughly 0.5 ppm error. Our results suggest that a monthly averaging period is generally useful for quantifying urban enhancements within 0.5 ppm. For 56 out of 72 site-months, the model-observation residual is less than 0.5 ppm. Further, only a few site-months considered had residuals significantly different from zero. The random errors associated with seasonal and yearly averaging times are less than 0.5 ppm, further supporting the model's usefulness for accurately quantifying urban enhancements from Indianapolis. The error at a yearly averaging period is particularly relevant to city GHG mitigation efforts because these goals are typically set at time periods of a year longer. Furthermore, the urban CO_2 enhancements of Indianapolis are relatively modest compared to larger cities; for cities with larger enhancements, the errors introduced by the model will be a smaller percentage of the overall urban enhancement. Given that the model is unbiased and the random errors at longer time spans are generally small relative to the impact of

urban emissions, we assert that VPRM is sufficient for representing biological CO_2 fluxes for inverse estimates of urban CO_2 emissions from Indianapolis.

While it is not essential for our application, we found that at a daily time scale, the model is not able to capture the observed differences in CO_2 mole fractions between background towers. The model-observation residuals at a daily time scale are often on the same order of magnitude as the observed enhancements themselves. The random error, as represented by the mean absolute error, at a daily scale is about 2.2 ppm, which is more than 50% of the 5 ppm average urban enhancement previously observed in Indianapolis. The inability of the model to capture the afternoon average CO_2 enhancements on a day-to-day basis may be due to transport error impacting the tower influence functions. Deng et al., (2017), documented day-to-day errors in wind direction in our atmospheric reanalysis on the order of 10 to 20 degrees. Transport errors like those described by Deng et al., (2017), could result in an incorrect estimation of surface influence for any particular hour, however, this would not bias the results over time.

In this study, we expanded upon the modeling work in Miles et al., (2021) in a number of ways. Most notable is our use of an improved VPRM formulation and new PFT parameter set developed by Gourdji et al., (2022). The present study uses a domain of roughly 300 km by 300 km, which includes the location of Tower 14, compared to the 87 km by 87 km domain used by Miles et al., (2021). Additionally, the influence functions used in this study include 72 hours back in time from the observation, while those used in Miles et al., (2021), include only 4 hours back in time. Another difference is that Miles et al., (2021), modeled both biological and anthropogenic impacts on the towers, while we evaluates only biological CO_2 fluxes.

Our evaluation of the differences in CO_2 mole fractions between Towers 01 and 09 agree with those of Miles et al., (2021), who suggested that the differences between growing season CO_2 mole fraction observations at Towers 01 and 09 can be attributed to the different predominant landcover types surrounding each tower (DBF at Tower 01 and agriculture at Tower

09). We determined that the dominant PFT within the influence area for Tower 01 is DBF, while the dominant PFT within the influence area for Tower 09 is Other Crops. Further, we found that the depletion of atmospheric CO_2 due to DBF is larger at Tower 01 compared to Tower 09, while Tower 09 has a larger depletion due to Other Crops and Corn PFTs compared to Tower 01.

The analysis presented in this study allowed us to further explore the potential causes of the differences in CO_2 mole fractions at Towers 09 and 14, which are both predominantly surrounded by agriculture. Miles et al., (2021), suggested that the differences may be due to a combination of a higher percentage of corn within a 10 km radius around Tower 14 compared to Tower 09 and a more productive harvest in the county Tower 14 resides in compared to Tower 09. In this study, we found that while Tower 14 does have more influence from corn compared to Tower 09, the influence from corn for each of the towers is too similar to account for the differences in CO_2 mole fraction between the sites. The model results presented here suggest that the differences in CO_2 mole fractions between Towers 09 and 14 are due to differences in corn productivity within the surface area influencing each tower (with the corn impacting Tower 14 having a higher productivity than that impacting Tower 09). This result both supports the hypothesis proposed by Miles et al., (2021), and shows that VPRM is able to capture observed differences in productivity within a single PFT category.

In addition to demonstrating VPRM's skill in replicating observed CO_2 mole fraction differences between background towers, we also found that VPRM is able to capture the large variability in the average daily cycle of CO_2 fluxes during the growing season across agricultural sites and years. The 2019 growing season was an atypical year for agriculture in the area due to extensive flooding during the spring and early summer which delayed planting (Yin et al., 2020). The effects of the delayed planting can be seen in the observations, with CO_2 drawdowns in July of that year being generally smaller than Julys of other years, with the exception of US-INn in 2019. It is particularly encouraging that the model was able to capture the observations for this

unusual year with similar skill (differences between modeled and observed peak drawdown of less than 30%) to the more typical years for four out of the five site-months during 2019. The one site-month that sticks out is US-INn during July 2019, which still has relatively high drawdown of CO_2. This site-month also sticks out because the model underestimates peak CO_2 drawdown by more than 50%. Given the model's ability to capture the observations during other site-months in 2019 with similar skill to other years, the unusual flooding and associated delayed planting cannot explain the larger difference between the observations and the model. A potential cause of this large difference could be in-field variability of productivity. The yield within a single agricultural field can vary significantly, however, this is outside the prediction ability of our roughly 1 km^2 resolution model.

Chapter 5

Conclusions

This study conducted a rigorous test of VPRM, a relatively simple and computationally inexpensive ecosystem CO_2 flux model, using the unique GHG observations available from the INFLUX network. We have shown that the model is able to capture observed differences in CO_2 mole fractions between INFLUX background towers without bias and with relatively small random errors when averaged over periods of a month or longer. This is particularly important given that VPRM has been used to represent biological CO_2 fluxes for inverse estimates of CO_2 emissions in previous studies. These results indicate that VPRM can reproduce CO_2 background conditions with an accuracy useful for long term monitoring of urban CO_2 enhancements from Indianapolis. Indianapolis is a moderately sized city on the edge of the US corn belt, with relatively small urban CO_2 enhancements compared to other larger cities, and strong ecosystem CO_2 fluxes due to the surrounding agriculture. VPRM's successful performance in this biologically active region is encouraging for the use of VPRM in other cities that may have larger CO_2 enhancements or less active biology.

We have presented an evaluation system that can be used to assess the performance of other ecosystem CO_2 flux models and can be applied to any city with a similar GHG monitoring network. The assessment of VPRM in other cities and regions should be a topic of further study. A challenge in some regions for the use of VPRM could be a lack of CO_2 flux observations for each region's common vegetation types; VPRM depends on CO_2 flux observations for parameterization of model PFTs, and this current study focuses on a region with a relative abundance of flux observations compared to other ecosystems around the globe.

References

Bakwin, P. S., Tans, P. P., Hurst, D. F., & Zhao, C. (1998). Measurements of carbon dioxide on very tall towers: results of the NOAA/CMDL program. *Tellus B: Chemical and Physical Meteorology*, 50:5, 401-415, DOI:10.3402/tellusb.v50i5.16216

C40 Cities. (n.d.). https://www.c40.org/

Davis, K. J., Deng, A., Lauvaux, T., Miles, N. L., Richardson, S. J., Sarmiento, D. P., Gurney, K. R., Hardesty, R. M., Bonin, T. A., Brewer, W. A., Lamb, B. K., Shepson, P. B., Harvey, R. M., Cambaliza, M. O., Sweeney, C., Turnbull, J. C., Whetstone, J., & Karion, A. (2017). The Indianapolis Flux Experiment (INFLUX): A test-bed for developing urban greenhouse gas emission measurements. *Elementa*, 5. https://doi.org/10.1525/elementa.188

Deng, A., Lauvaux, T., Davis, K. J., Gaudet, B. J., Miles, N., Richardson, S. J., Wu, K., Sarmiento, D. P., Hardesty, R. M., Bonin, T. A., Brewer, W. A., & Gurney, K. R. (2017). Toward reduced transport errors in a high resolution urban CO_2 inversion system. *Elementa*, 5. https://doi.org/10.1525/elementa.133

Dewitz, J., and U.S. Geological Survey. (2021). National Land Cover Database (NLCD) 2019 Products (ver. 2.0, June 2021): U.S. Geological Survey data release, https://doi.org/10.5066/P9KZCM54

Didan, K. (2015a). MOD13A2 MODIS/Terra Vegetation Indices 16-Day L3 Global 1km SIN Grid V006 [Data set]. NASA EOSDIS Land Processes DAAC. Accessed 2022-10-15 from https://doi.org/10.5067/MODIS/MOD13A2.006

Didan, K. (2015b). MYD13A2 MODIS/Aqua Vegetation Indices 16-Day L3 Global 1km SIN Grid V006 [Data set]. NASA EOSDIS Land Processes DAAC. Accessed 2022-10-15 from https://doi.org/10.5067/MODIS/MYD13A2.006

Foken, T. (2008). Micrometeorology (Carmen J. Nappo). *Springer*.

Global Covenant of Mayors for Climate & Energy. (n.d.). https://www.globalcovenantofmayors.org/

Gourdji, S. M., Karion, A., Lopez-coto, I., Ghosh, S., Mueller, K. L., Zhou, Y., Williams, C. A., Baker, I. T., Haynes, K. D., & Whetstone, J. R. (2022). A Modified Vegetation Photosynthesis and Respiration Model (VPRM) for the Eastern USA and Canada, Evaluated With Comparison to Atmospheric Observations and Other Biospheric Models. *Journal of Geophysical Research: Biogeosciences*. https://doi.org/10.1029/2021JG006290

Gurney, K. R., Razlivanov, I., Song, Y., Zhou, Y., Benes, B., & Abdul-Massih, M. (2012). Quantification of fossil fuel CO_2 emissions on the building/street scale for a large U.S. City. *Environmental Science and Technology*, 46(21), 12194–12202. https://doi.org/10.1021/es3011282

Horne, J., Davis, K., Miles., N., Richardson, S., Haupt, B., Foust, E., Kenion, H., & Murphy, S. (in prep). Urban Eddy Covariance – The INFLUX Network.

Karion, A., Callahan, W., Stock, M., Prinzivalli, S., Verhulst, K. R., Kim, J., Salameh, P. K., Lopez-Coto, I., & Whetstone, J. (2020). Greenhouse gas observations from the Northeast Corridor tower network. *Earth Syst. Sci. Data*, 12, 699–717, https://doi.org/10.5194/essd-12-699-2020

Karion, A., Lopez-Coto, I., Gourdji, S. M., Mueller, K., Ghosh, S., Callahan, W., Stock, M., Digangi, E., Prinzivalli, S., & Whetstone, J. (2021). Background conditions for an urban greenhouse gas network in the Washington, DC, and Baltimore metropolitan region. *Atmospheric Chemistry and Physics*, 21(8), 6257–6273. https://doi.org/10.5194/acp-21-6257-2021

King, C., (2021, March 18). Our year of COVID: Key dates in Indiana's fight against the coronavirus. *Indy Star*. https://www.indystar.com/in-

depth/news/2021/03/18/indiana-covid-timeline-key-dates-states-fight-vs-pandemic/6813412002/

Kljun, N., Calanca, P., Rotach, M. W., & Schmid, H. P. (2015). A simple two-dimensional parameterisation for Flux Footprint Prediction (FFP). *Geoscientific Model Development*, 8(11), 3695–3713. https://doi.org/10.5194/gmd-8-3695-2015

Lauvaux, T., Miles, N. L., Deng, A., Richardson, S. J., Cambaliza, M. O., Davis, K. J., Gaudet, B., Gurney, K. R., Huang, J., O'Keefe, D., Song, Y., Karion, A., Oda, T., Patarasuk, R., Razlivanov, I., Sarmiento, D., Shepson, P., Sweeney, C., Turnbull, J., & Wu, K. (2016). High-resolution atmospheric inversion of urban CO_2 emissions during the dormant season of the Indianapolis flux experiment (INFLUX). *Journal of Geophysical Research*, 121(10), 5213–5236. https://doi.org/10.1002/2015JD024473

Lauvaux, T., Gurney, K. R., Miles, N. L., Davis, K. J., Richardson, S. J., Deng, A., Nathan, B. J., Oda, T., Wang, J. A., Hutyra, L., & Turnbull, J. (2020). Policy-relevant assessment of urban CO_2 emissions. *Environmental Science and Technology*, 54(16), 10237–10245. https://doi.org/10.1021/acs.est.0c00343

Lwasa, S., Seto, K.C., Bai, X., Blanco, H., Gurney, K. R., Kılkış, Ş., Lucon, O., Murakami, J., Pan, J., Sharifi, A., & Yamagata, Y. (2022). Urban systems and other settlements. In IPCC, 2022: Climate Change 2022: Mitigation of Climate

Change. Contribution of Working Group III to the Sixth Assessment Report of the Intergovernmental Panel on Climate Change [Shukla, P. R., Skea, J., Slade, R., Al Khourdajie, A., van Diemen, R., McCollum, D., Pathak, M., Some, S., Vyas, P., Fradera, R., Belkacemi, M., Hasija, A., Lisboa, G., Luz, S., & Malley, J. (eds.)]. Cambridge University Press, Cambridge, UK and New York, NY, USA. doi:10.1017/9781009157926.010

Mahadevan, P., Wofsy, S. C., Matross, D. M., Xiao, X., Dunn, A. L., Lin, J. C., Gerbig, C., Munger, J. W., Chow, V. Y., & Gottlieb, E. W. (2008). A satellite-based biosphere parameterization for net ecosystem CO_2 exchange: Vegetation Photosynthesis and Respiration Model (VPRM). *Global Biogeochemical Cycles*, 22(2). https://doi.org/10.1029/2006GB002735

McKain, K., Wofsy, S. C., Nehrkorn, T., Eluszkiewicz, J., Ehleringer, J. R., & Stephens, B. B. (2012). Assessment of ground-based atmospheric observations for verification of greenhouse gas emissions from an urban region. *Proceedings of the National Academy of Sciences of the United States of America*, 109(22), 8423–8428. https://doi.org/10.1073/pnas.1116645109

Miles, N. L., Richardson, S. J., Lauvaux, T., Davis, K. J., Deng, A., Turnbull, J., Karion, A., Sweeney, C., Gurney, K. R., Patarasuk, R., Razlivanov, I., Cambaliza, M. O., & Shepson, P. B., (2017). Quantification of urban atmospheric boundary layer greenhouse gas dry mole fraction enhancements: Results from the Indianapolis

Flux Experiment (INFLUX), *Elem Sci Anth*., 5:27. http://doi.org/10.1525/elementa.127

Miles, N. L., Davis, K. J., Richardson, S. J., Lauvaux, T., Martins, D. K., Deng, A. J., Balashov, N., Gurney, K. R., Liang, J., Roest, G., Wang, J. A., & Turnbull, J. C. (2021). The influence of near-field fluxes on seasonal carbon dioxide enhancements: results from the Indianapolis Flux Experiment (INFLUX). *Carbon Balance and Management*, 16(1), 1–15. https://doi.org/10.1186/s13021-020-00166-z

Mitchell, L., Lin, J., Hutyra, L., Bowling, D., Cohen, R., Davis, K., Digangi, E., Duren, R., Ehleringer, J., Fain, C., Falk, M., Guha, A., Karion, A., Keeling, R., Kim, J., Miles, N., Miller, C., Newman, S., Pataki, D., Prinzivalli, S., Ren, X., Rice, A., Richardson, S., Sargent, M., Stephens, B., Turnbull, J., Verhulst, K., Vogel, F., Weiss, R., Whetstone, J., & Wofsy, S., (2022). A Multi-City Urban Atmospheric Greenhouse Gas Measurement Data Synthesis. *Scientific Data*, 9, 1, 361, https://doi.org/10.1038/s41597-022-01467-3

Mueller, K., Yadav, V., Lopez-Coto, I., Karion, A., Gourdji, S., Martin, C., & Whetstone, J. (2018). Siting Background Towers to Characterize Incoming Air for Urban Greenhouse Gas Estimation: A Case Study in the Washington, DC/Baltimore Area. *Journal of Geophysical Research: Atmospheres*, 123(5), 2910–2926. https://doi.org/10.1002/2017JD027364

National Weather Service Automated Surface Observing Systems (ASOS). https://www.weather.gov/asos/

Rice, A., & Bostrom, G. (2011). Measurements of carbon dioxide in an Oregon metropolitan region. *Atmospheric Environment*, 45(5), 1138–1144. https://doi.org/10.1016/j.atmosenv.2010.11.026

Richardson, S. J., Miles, N. L., Davis, K. J., Lauvaux, T., Martins, D. K., Turnbull, J. C., McKain, K., Sweeney, C., & Cambaliza, M. O. L. (2017). Tower measurement network of in-situ CO_2, CH_4, and CO in support of the Indianapolis FLUX (INFLUX) Experiment. *Elementa*, 5. https://doi.org/10.1525/elementa.140

Sargent, M., Barrera, Y., Nehrkorn, T., Hutyra, L. R., Gately, C. K., Jones, T., McKain, K., Sweeney, C., Hegarty, J., Hardiman, B., Wang, J. A., & Wofsy, S. C. (2018). Anthropogenic and biogenic CO_2 fluxes in the Boston urban region. *Proceedings of the National Academy of Sciences of the United States of America*, 115(29), 7491–7496. https://doi.org/10.1073/pnas.1803715115

Shusterman, A. A., Teige, V. E., Turner, A. J., Newman, C., Kim, J., & Cohen, R. C. (2016). The BErkeley Atmospheric CO_2 Observation Network: initial evaluation. *Atmos. Chem. Phys.*, 16, 13449–13463, https://doi.org/10.5194/acp-16-13449-2016

Staufer, J., Broquet, G., Bréon, F.-M., Puygrenier, V., Chevallier, F., Xueref-Rémy, I., Dieudonné, E., Lopez, M., Schmidt, M., Ramonet, M., Perrussel, O., Lac, C., Wu, L., & Ciais, P. (2016). The first 1-year-long estimate of the Paris region fossil fuel CO_2 emissions based on atmospheric inversion. *Atmos. Chem. Phys.*, 16, 14703–14726, https://doi.org/10.5194/acp-16-14703-2016

Turnbull, J. C., Sweeney, C., Karion, A., Newberger, T., Lehman, S. J., Tans, P. P., Davis, K. J., Lauvaux, T., Miles, N. L., Richardson, S. J., Cambaliza, M. O., Shepson, P. B., Gurney, K., Patarasuk, R., & Razlivanov, I. (2015). Toward quantification and source sector identification of fossil fuel CO_2 emissions from an urban area: Results from the INFLUX experiment. *Journal of Geophysical Research*, 120(1), 292–312. https://doi.org/10.1002/2014JD022555

Turnbull, J. C., Karion, A., Davis, K. J., Lauvaux, T., Miles, N. L., Richardson, S. J., Sweeney, C., McKain, K., Lehman, S. J., Gurney, K. R., Patarasuk, R., Liang, J., Shepson, P. B., Heimburger, A., Harvey, R., & Whetstone, J. (2019). Synthesis of Urban CO_2 Emission Estimates from Multiple Methods from the Indianapolis Flux Project (INFLUX). *Environmental Science and Technology*, 53(1), 287–295. https://doi.org/10.1021/acs.est.8b05552

Uliasz, M. (1994). Environmental Modelling II; Computational Mechanics Publications: Southampton, U.K., pp 71−102.

U.S. Census Bureau. (2022). Population Estimates, July 1, 2022 (V2022) -- Indianapolis city, Indiana [data table]. Quick Facts. https://www.census.gov/quickfacts/fact/table/indianapoliscitybalanceindiana/PST045222#qf-flag-NA

USDA National Agricultural Statistics Service (NASS) Cropland Data Layer. Published crop-specific data layer [Online]. Available at https://croplandcros.scinet.usda.gov/ USDA-NASS, Washington, DC.

Verhulst, K. R., Karion, A., Kim, J., Salameh, P. K., Keeling, R. F., Newman, S., Miller, J., Sloop, C., Pongetti, T., Rao, P., Wong, C., Hopkins, F. M., Yadav, V., Weiss, R. F., Duren, R. M., & Miller, C. E. (2017). Carbon dioxide and methane measurements from the Los Angeles Megacity Carbon Project - Part 1: Calibration, urban enhancements, and uncertainty estimates. *Atmospheric Chemistry and Physics*, 17(13), 8313–8341. https://doi.org/10.5194/acp-17-8313-2017

Vermote, E. (2015a). MOD09A1 MODIS/Terra Surface Reflectance 8-Day L3 Global 500m SIN Grid V006 [Data set]. NASA EOSDIS Land Processes DAAC. Accessed 2022-10-15 from https://doi.org/10.5067/MODIS/MOD09A1.006

Vermote, E. (2015b). MYD09A1 MODIS/Aqua Surface Reflectance 8-Day L3 Global 500m SIN Grid V006 [Data set]. NASA EOSDIS Land Processes DAAC. Accessed 2022-10-15 from https://doi.org/10.5067/MODIS/MYD09A1.006

Vickers, D., & Mahrt, L. (1997). Quality control and flux sampling problems for tower and aircraft data. *Journal of Atmospheric and Oceanic Technology*, 14(3), 512–526. https://doi.org/10.1175/1520-0426(1997)014<0512:QCAFSP>2.0.CO;2

Vogel, F.R., Ishizawa, M., Chan, E., Chan, D., Hammer, S., Levin, I., & Worthy, D.E.J. (2012). Regional non-CO_2 greenhouse gas fluxes inferred from atmospheric measurements in Ontario, Canada. *Journal of Integrative Environmental Sciences*, 9:sup1, 41-55, DOI:10.1080/1943815X.2012.691884

Wu, K., Lauvaux, T., Davis, K. J., Deng, A., Coto, I. L., Gurney, K. R., & Patarasuk, R. (2018). Joint inverse estimation of fossil fuel and biogenic CO_2 fluxes in an urban environment: An observing system simulation experiment to assess the impact of multiple uncertainties. *Elementa*, 6. https://doi.org/10.1525/elementa.138

Yin, Y., Byrne, B., Liu, J., Wennberg, P. O., Davis, K. J., Magney, T., Köhler, P., He, L., Jeyaram, R., Humphrey, V., Gerken, T., Feng, S., Digangi, J. P., & Frankenberg, C. (2020). Cropland Carbon Uptake Delayed and Reduced by 2019 Midwest Floods. *AGU Advances*, 1(1). https://doi.org/10.1029/2019av0001